

Supporting Information

JACS Communication

Molecular Logic Gates Using Surface-Enhanced Raman Scattered Light

Edward H. Witlicki, Carsten Johnsen, Stinne W. Hansen, Daniel W. Silverstein,
Vincent J. Bottomley, Jan O. Jeppesen, Eric W. Wong, Lasse Jensen, and Amar H. Flood

Table of Contents

- S1. General Experimental Methods**
- S2. Preparation of MPTTF**
- S3. Spectroscopy and Characterization of the Host-Guest Complexation**
- S4. Construction of the Three-electrode Cell**
- S5. UV-Vis-NIR Spectroelectrochemistry of MPTTF**
- S6. Solution-phase Raman Spectroelectrochemistry**
- S7. SERS Enhancements from Flat Gold and Nanodisc Arrays**
- S8. Electrodynamics Simulations**
- S9. Complete Reference 11b**
- S10. References**

S1. General Experimental Methods. Acetonitrile was purchased from commercial sources and freshly distilled over CaH₂ before use, while DMF was allowed to stand over molecular sieves (4 Å) for at least 3 days prior to use. 2-[4,5-Bis(methylthio)-1,3-dithiole-2-ylidene]-(1,3)-dithiolo[4,5-*c*]pyrrole^{S1} and cyclobis(paraquat-*p*-phenylene) tetrakis(hexafluorophosphate)^{S2} (CBPQT•4PF₆) were prepared accordingly to literature procedures. Melting points (M.p.) were determined on a Büchi melting point apparatus and are uncorrected. ¹H NMR and ¹³C NMR spectra were recorded at room temperature at 300 MHz and 75 MHz, respectively, on a Gemini-300BB instrument using residual non-deuterated solvent as the internal standard. The solvent signals were assigned by Nudelman.^{S3} All chemical shifts are quoted on a δ scale, and all coupling constants (*J*) are expressed in Hertz (Hz). The following abbreviations are used in listing the NMR spectra: s = singlet, bs = broad singlet, d = doublet, t = triplet, q = quartet, and m = multiplet. Samples were prepared using CDCl₃, CD₃CN, or CD₃SOCD₃ purchased from Cambridge Isotope Labs or Sigma-Aldrich. Electrospray ionization mass spectrometry (ESI-MS) was performed on a Thermo Finnigan MAT SSQ710 single stage quadrupole mass spectrometer. UV-Vis-NIR spectra were collected using a Varian Cary 5000 spectrometer. Raman spectra were recorded on a InVia Renishaw Raman Microscope diode laser with 785 nm excitation and Raman shift positions were calibrated to the 520.5 cm⁻¹ band of silicon. Spectra were baseline corrected where appropriate. Spectra were recorded using a 50 \times , numerical aperture (NA) = 0.7 objective lens focused into solutions or onto nanodisc array surfaces. Solutions were contained in 1 cm cuvettes obtained Starna (type 21/Q/1, Spectrosil[®] quartz). Electrochemistry was performed using a Princeton Applied Electronics potentiostat model 263A. Elemental analysis was performed by the Atlantic Microlabs, Inc., Atlanta, Georgia.

S2. Preparation of 2-[4,5-bis(methylthio)-1,3-dithiole-2-ylidene]-5-(prop-2-yn-1-yl)-(1,3)-dithiolo[4,5-*c*]pyrrole (MPTTF). A solution of 2-[4,5-bis(methylthio)-1,3-dithiole-2-ylidene]-(1,3)-dithiolo[4,5-*c*]pyrrole (0.350 g, 1.04 mmol) in anhydrous DMF (10 mL) was degassed for 15 min with argon before a suspension of NaH in mineral oil (55 w/w %, 0.228 g, 5.23 mmol) was added in one portion. Subsequently, a solution of propargylic bromide in toluene (80 w/w %, 0.13 mL, 0.174 g, 1.17 mmol) was added, whereafter the reaction mixture was stirred under argon at room temperature for 1 h. The reaction was terminated by addition of brine (50 mL) and the resulting mixture was extracted with CH₂Cl₂ (4 \times 50 mL). The combined organic phases were dried (MgSO₄) and the solvent was removed in vacuo. The resulting residue was purified by column chromatography (SiO₂, CH₂Cl₂/petroleum ether v/v 1:3) yielding the product MPTTF as a yellow solid (0.230 g, 59%): mp 102–104°C; ¹H NMR (CDCl₃, 300 MHz) δ 2.43 (s, 6H), 2.46 (t, *J* = 4 Hz, 1H) 4.61 (d, *J* = 4 Hz, 2H), 6.58 (s, 2H); ¹³C NMR (CDCl₃, 75 MHz) δ 19.3, 39.8, 74.6, 77.4, 110.8, 112.4, 120.1, 120.7, 127.3; MS(ESI) *m/z* 197 (100), 373 ([M]⁺, 66), 396 ([M + Na]⁺, 65); MS (HiResESI), calcd for C₁₃H₁₁NNaS₆⁺ 395.9109; found 395.9112. Anal. Calcd. for C₁₃H₁₁NS₆: C, 41.79; H, 2.97; N, 3.75; S, 51.49. Found: C, 42.38; H, 2.92; N, 3.55; S, 50.67.

S3. Spectroscopy and Characterization of the Host-Guest Complexation. The host-guest complexation was examined (Figure S1) using UV-Vis-NIR and resonance Raman scattering (RRS) spectroscopy. Titration of the MPTTF thread into a solution of the CBPQT⁴⁺ generated a characteristic charge-transfer (CT) absorption band at 810 nm (ϵ = 2100 M⁻¹ cm⁻¹, MeCN). The UV-Vis-NIR titration curve was fitted using the simulation software Sivvu^{S4} to generate a binding constant of K_a = 28,000 \pm 1,000 M⁻¹ (ΔG_a = -6.07 \pm 0.03 kcal mol⁻¹). The same solution

was examined using 785 nm laser excitation, which is resonant with the CT chromophore. Consequently, a series of RRS spectra (Figure S1c) were generated showing bands that are characteristic of the CT chromophore growing in concomitantly with additions of MPTTF. The bands match well with the RRS spectrum generated by the TTFCCBPQT⁴⁺ complex^{S5} corroborating the assignment. The main difference is the enhancement of an additional band at 1521 cm⁻¹, which is assigned as a pyrrole-based vibration. Using a 1:1 binding model^{S6} for fitting the RRS band intensities generates an average binding constant of $K_a = 39,000 \pm 1,000 \text{ M}^{-1}$ ($\Delta G_a = -6.3 \pm 0.4 \text{ kcal mol}^{-1}$).

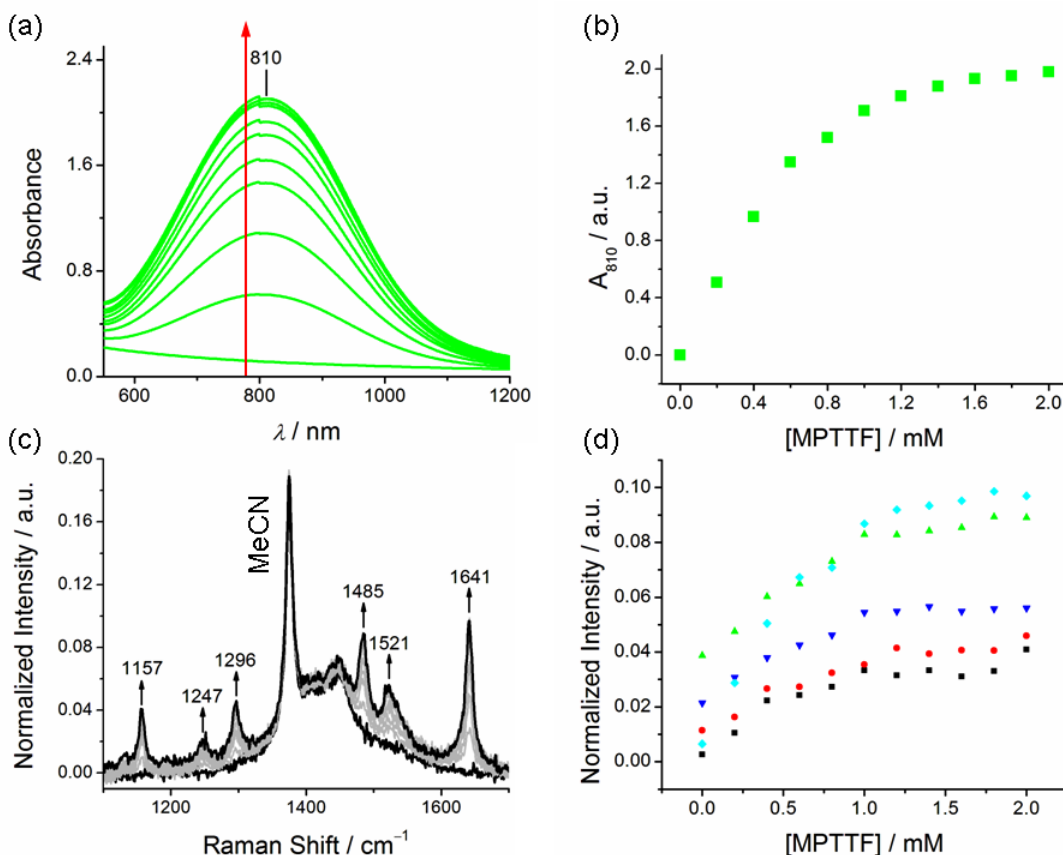


Figure S1. Titration of MPTTF into a solution of CBPQT⁴⁺ (1 mM, MeCN, 298 K) characterized by (a) UV-Vis-NIR and (c) resonance Raman scattering spectroscopy. Binding curves are shown for (b) $\lambda_{\text{max}} = 810 \text{ nm}$ and (d) for selected Raman vibrational bands.

S4. Construction of the Three-electrode Cell

The SERS spectroelectrochemistry (SEC) cell was constructed by modifying a wafer cartridge assembly.^{S7} Channels were drilled into the Teflon cartridge for running electrodes through to the solution (Figure S2a). The Ag/AgCl reference electrode (Figure S2a, blue line) was prepared from a silver wire such that only the tip was coated in AgCl; the remaining silver was insulated from solution by wrapping Teflon tape around the wire. The reference electrode was then oriented just under the working electrode. The working electrode was prepared from a Pt wire with a flattened end strapped over a wafer with nanodisc arrays seated in the cartridge recess.

The flattened Pt was then tied down with strings of Teflon (Figure S2b). Once this piece was assembled, it was lowered into the cuvette containing the analyte solution, and a counter electrode (coiled Pt wire) was lowered into the solution above the cartridge (Figure S2c). The other ends of the electrodes were put through a septum, which was used to seal the cell.

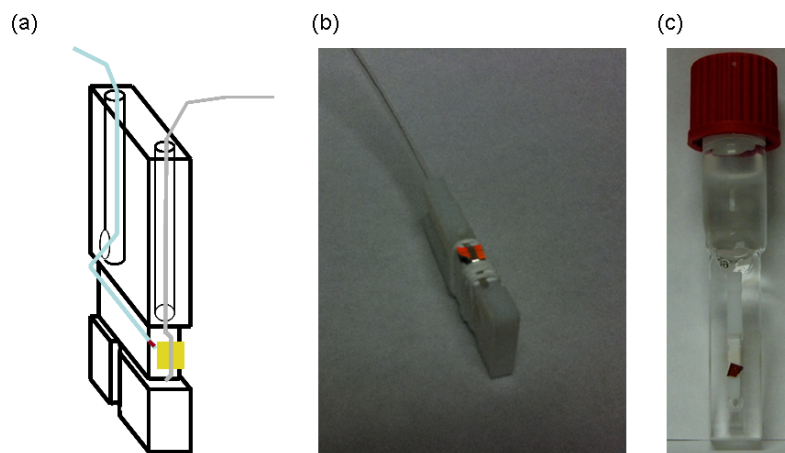


Figure S2. (a) A schematic model of the apparatus setup for creating thin film solutions (path length $<1 \mu\text{m}$) over the nanodisc arrays interfaced with a potentiostat, (b) photographs of the wafer strapped with the flattened end of a Pt wire, and (c) the entire assembly.

S5. UV-Vis-NIR Spectroelectrochemistry of MPTTF

UV-Vis-NIR spectroelectrochemical spectra (Figure S3) were collected from a solution of MPTTF contained in a three-electrode quartz cell with a 1 mm path length placed in the Cary 5000 UV-Vis-NIR spectrophotometer. The potential was stepped to +0.6 V to generate MPTTF^+ and the instrument was set to scan repeatedly. Electrolysis of the solution was achieved when the intensity of the spectrum stopped changing (~ 5 minutes). The voltage was then stepped to +0.9 V and the solution scanned until electrolysis was once again achieved. The spectra exhibiting maximum intensities were used for display (Figure 1 in the main text and Figure S3).

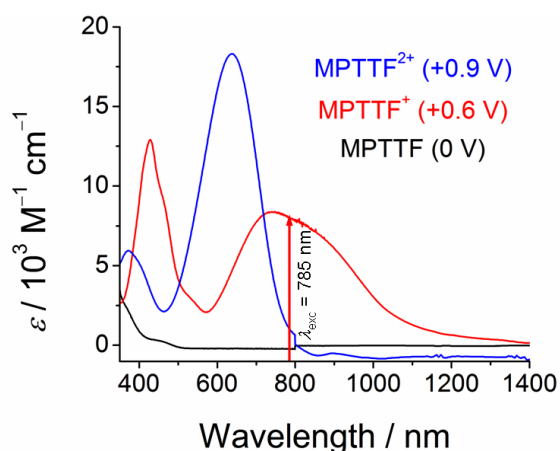


Figure S3. UV-Vis-NIR SEC extinction spectra of MPTTF (black trace), MPTTF^+ (red trace), and MPTTF^{2+} (red trace). Conditions: 1 mM MPTTF, MeCN, 298 K, potentials vs. Ag/AgCl, 0.1 M TBAPF₆.

S6. Solution-phase Raman Spectroelectrochemistry

Solution-phase spectra of the oxidized states were collected using spectroelectrochemistry from a three-electrode cell. A modified 1 mm path length quartz cuvette was used for the cell. The working electrode was fabricated from a platinum mesh with a small pinhole in its center where the Raman excitation laser (785 nm) was focused in order to obtain spectra from the electrolyzed solution. The counter electrode (coiled platinum wire), was situated above the working electrode. The reference electrode was made from a silver wire coated with AgCl and insulated with Teflon tape with its tip exposed. The tip of the reference electrode was placed close to the working electrode.

A solution of the complex was prepared with the same concentrations as those used in the SERS-SEC experiment (600 μM CBPQT⁴⁺, 200 μM MPTTF, 0.1 M TBAPF₆, MeCN). The spectrum collected with an applied voltage of 0 V (Figure S4, green trace) shows weak signals from the complex, which is expected at these concentrations. The potential was stepped to +0.6 V to generate and collect spectra of MPTTF⁺ (Figure S4, red trace) and then to +0.9 V for MPTTF²⁺ (Figure S4, blue trace).

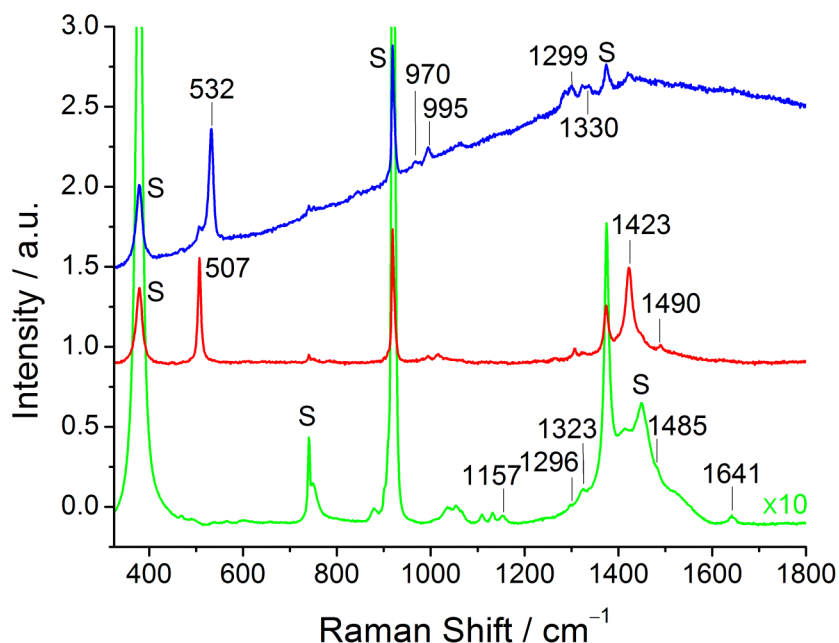


Figure S4. Raman SEC spectra for the MPTTF/CBPQT⁴⁺ complex (~186 μM , green), MPTTF⁺ (red), and MPTTF²⁺ (blue) in solution. Conditions: $\lambda_{\text{exc}} = 785$ nm, 30 mW, 50 \times objective (NA = 0.7), 10 s exposure time, average of 10 (red and blue traces) or 100 (green trace) spectra. Solvent bands are marked with an S.

S7. SERS Enhancements from Flat Gold and Nanodisc Arrays.

In order to understand the enhancement mechanisms at play for each species in the vicinity of the nanodisc array, several Raman spectroelectrochemistry experiments were performed. Spectra obtained from thin films of solution in contact with flat gold and the nanodisc array as well as from bulk solutions. The complex was examined at ~186 μM while the experiments using the

MPTTF thread alone were performed at a much lower concentration (20 μM) in order to obtain better intensity contrast when comparing solution spectra with surface spectra.

For the complex $\text{MPTTF} \cdot \text{CBPQT}^{4+}$, the intensity pattern seen from bulk solution (Figure S5a, blue trace) is typical^{S5} of resonance with the charge-transfer chromophore of TTF-based complexes with CBPQT^{4+} . The same overall intensity pattern is seen from the nanodisc array (Figure S5c, green trace), meaning that this spectrum is resonant in nature. The scaled intensities generated from the nanodisc array are greatly enhanced when compared to solution, indicating that surface enhancement also plays a role in determining the enhancement. Molecular adsorption often plays important roles in surface enhancement on account of the fact that it can lead to preconcentration of the sample and it brings the analyte into the plasmonic field. In the case of the complex, the SERS spectra show small wavenumber shifts in the Raman bands indicating some degree of surface adsorption is present. Interestingly, the absence of any Raman intensity from the flat gold (Figure S5b, red trace) indicates preconcentration is not contributing as much as the plasmonic field to the surface enhancement. Taken together – the resonant signature and surface enhancements – the spectrum from the complex is assigned as a resonant SERS spectrum, i.e., SERRS.

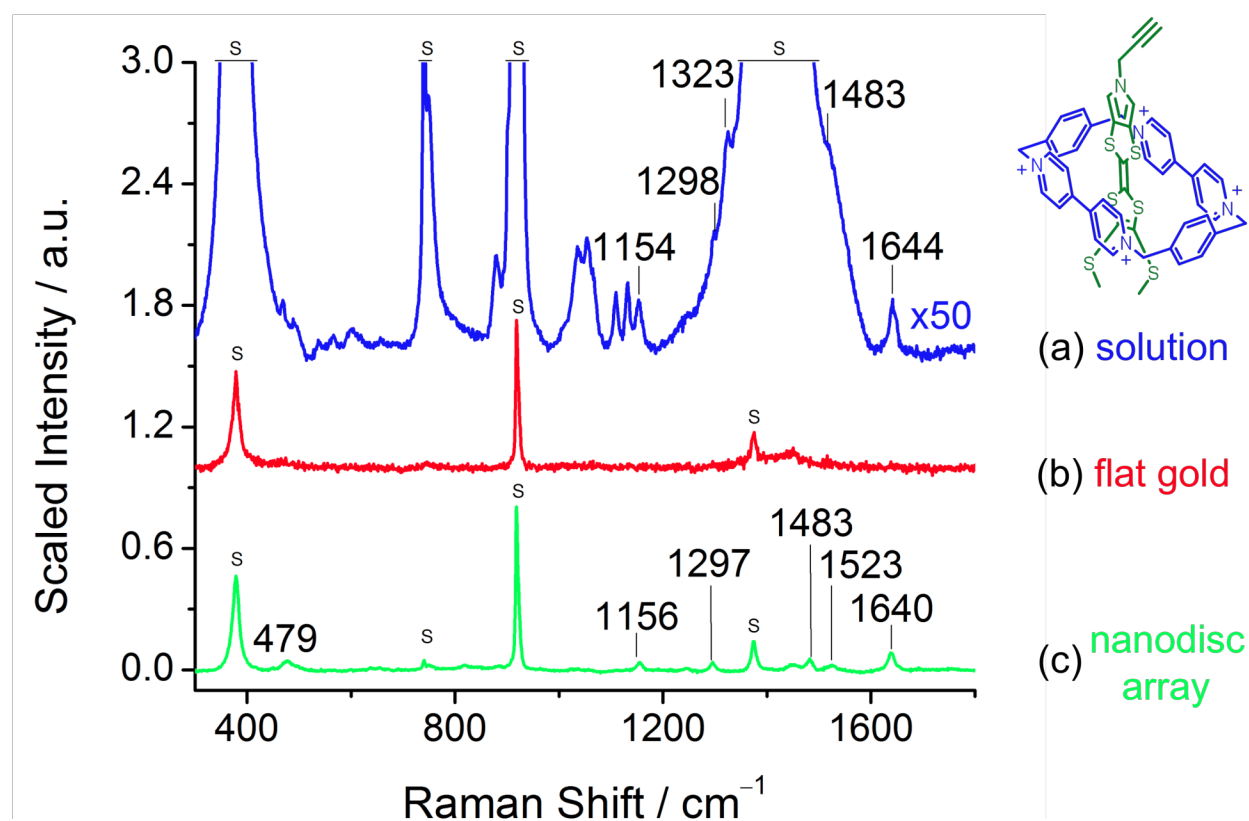


Figure S5. Raman spectra ($\lambda_{\text{exc}} = 785 \text{ nm}$) of (a) the $\text{MPTTF} \cdot \text{CBPQT}^{4+}$ complex (200 μM MPTTF + 600 μM CBPQT^{4+}) obtained from bulk solution (blue trace), (b) a thin solution film over flat gold (red trace) and (c) a thin solution film over the nanodisc array (green trace). Conditions: MeCN, 298 K, average of 5 spectra collected over 10 s using 30 mW laser power. The spectrum of the solution of the complex in (a) (blue trace) is an average of 1000 spectra under the same conditions as the others. Solvent bands are marked with an S.

Examination of spectra from the neutral MPTTF in solution, from flat gold and the nanodisc array (Figure S6a) shows no intensity anywhere.

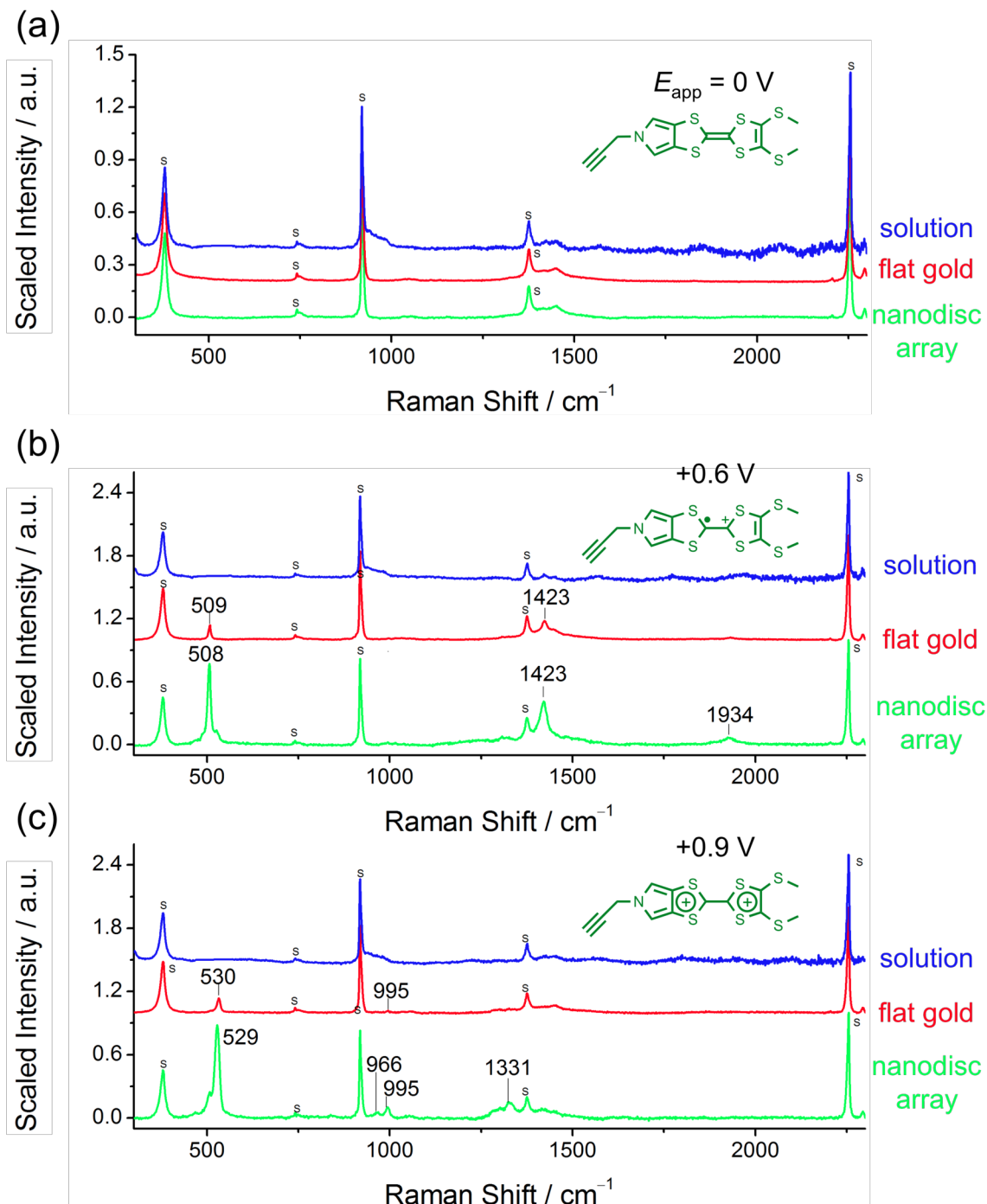


Figure S6. Raman-SEC spectra of an MPTTF solution (20 μ M MPTTF) in the SEC cell are shown at potentials of (a) 0 V (neutral MPTTF), (b) +0.6 V (MPTTF⁺) and (c) +0.9 V (MPTTF²⁺). Conditions: Average of 5 spectra collected over 10 s using 30 mW laser power, potentials vs. Ag/AgCl, other conditions are the same as in Figure S5. Solvent bands are marked with an S.

Raman spectra of the MPTTF^+ monocation at $20 \mu\text{M}$ (Figure S6b) shows no Raman activity from bulk solution under the experimental conditions. By contrast, spectra from both flat gold and the nanodisc array display characteristic Raman bands of MPTTF^+ . Furthermore, their intensity patterns are the same as those recorded in solution at a higher concentration ($200 \mu\text{M}$, Figure S4, red trace), indicating that the SERS spectra of MPTTF^+ are also resonant in nature. Unlike the complex (Figure S5b), a significant signal from the monocation is produced from flat gold, which is indicative of surface adsorption contributing to enhancement, whether by preconcentration and/or some other plasmonic contribution. Comparing the spectrum from flat gold to that of the nanodisc array, all signals of the monocation are further enhanced. These observations indicate that the spectrum from the nanodisc array is a resonant SERS spectrum and that surface adsorption plays an important role in the enhancement.

For the MPTTF^{2+} dication (Figure S6c), no Raman signals are seen from solution, and while spectra are observed from flat gold and the nanodisc array, they show different intensity profiles. The peak locations and intensity pattern from the array are also similar to those found in solution at a higher concentration (Figure S4, blue trace). Unlike the complex or the monocation, MPTTF^{2+} lacks a chromophore resonant with the excitation laser (Figure S4, blue trace), and so the enhancements seen from the gold surfaces are also attributed to surface adsorption. The spectrum from the nanodisc array is also enhanced compared to flat gold. These observations are consistent with surface enhancement where adsorption of MPTTF^{2+} places it inside the plasmonic. Thus, the spectrum from the nanodisc array is a normal SERS spectrum and surface adsorption plays an important role in the mode of enhancement.

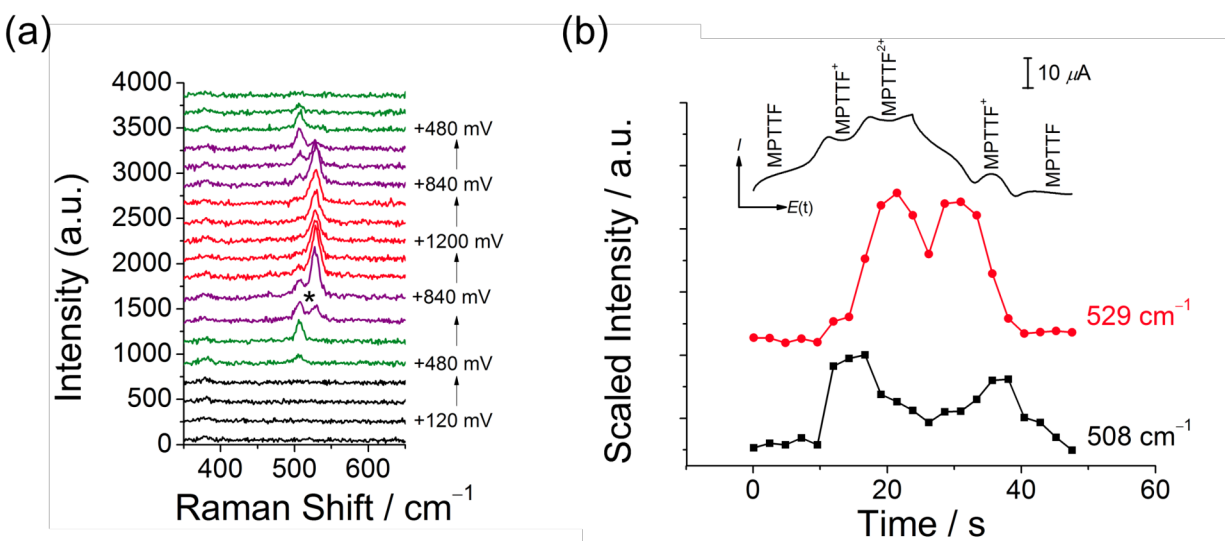


Figure S7. (a) The lower wavenumber region of SERS spectra collected during a CV experiment from a thin solution film over the nanodisc array (2.8 s per spectrum, 50.5 mV s^{-1} , $E_i = 0 \text{ V}$, $E_f = +1.2 \text{ V}$, other conditions same as in Figure S5). (b) Stacked CV current response and normalized SERS peak intensities vs. time traces for MPTTF^+ (508 cm^{-1} , black trace) and MPTTF^{2+} (529 cm^{-1} , red trace).

The scattered light for MPTTF^+ (508 cm^{-1}) and MPTTF^{2+} (521 cm^{-1}) are very close in wavelength (819 and 818 nm, respectively), which creates a situation in which the possibility for cross-talk effects are a concern. However, the resolving power of the spectrometer in this case is less than $\pm 1\text{ cm}^{-1}$, or $\pm 0.07\text{ nm}$. In the situation where the two bands are of the same intensity during the transition from the monocation to the dication, the resolution is sufficient enough to clearly resolve the two peaks (Figure S7, see asterisk). It is also important to note that the manuscript describes the voltage input in terms of the inputs $0x$, $1x$ and $2x$, where $x = +0.6\text{ V}$. The CV experiments used in the manuscript had a vertex potential of $+0.9\text{ V}$. While $2x$ does not give the input of $+0.9\text{ V}$ (but rather $+1.2\text{ V}$), the spectral response is the same (Figure S7). One feature that does not appear in the manuscript as it does in this example is the decrease in SERS intensity for MPTTF^{2+} (529 cm^{-1}) that is due to diffusion effects (this decrease corresponds well to the current response of the CV in the same region).

On the basis of these spectral features, an equivalent circuit and series of logic operations were conceived (Figure S8).

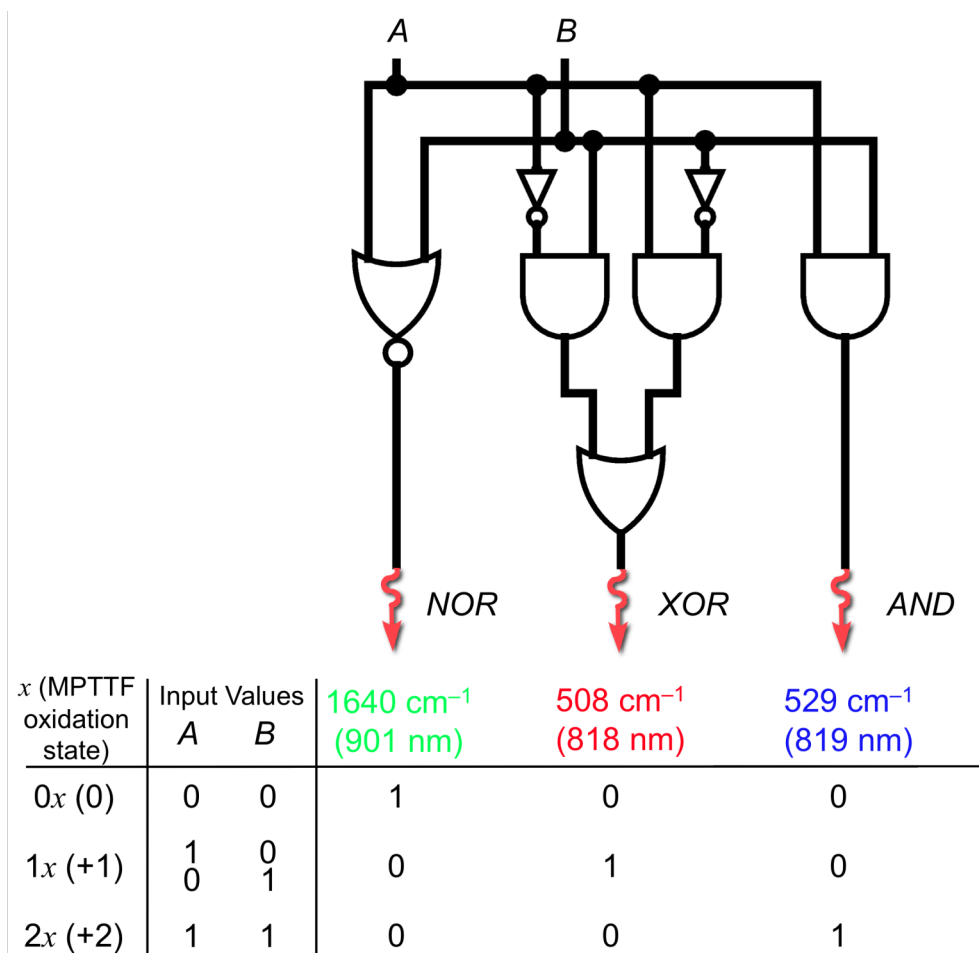


Figure S8. A logic gate series and truth table representing the optical output of the MPTTFCCBPQT^{4+} system from three different values of x ($x = +0.6\text{ V}$).

S8. Electrodynamic Simulations

The ground state equilibrium geometries and normal modes for the molecules were determined using the B3LYP functional and 6-311G* basis set, except for the MPTTFCCBPQT⁴⁺ complex where the 6-31G* basis set was used. The B3LYP frequencies were scaled by 0.98 as is typical. Optical properties, including the excited state energies that were used for determining the dimensionless displacements, were calculated using the time-dependent density functional theory (TDDFT) linear response method with the 6-311G* basis set for all molecules. The dimensionless displacements were calculated based on the B3LYP geometries and B3LYP normal modes by using LC- ω PBEh functional for calculating the excitation energies.^{S8} LC- ω PBEh functionals belong to the class of long-range corrected DFT functionals that have been shown to provide accurate excitation energies. All calculations were done using the recent implementation of long-range corrected DFT functionals into the NWChem program package.^{S9}

The resonance Raman scattering (RRS) spectra were simulated using Heller's time-dependent theory as:^{S9c,S10}

$$\alpha_{\alpha\beta} = \sum_n \mu_{\alpha}^{0n} \mu_{\beta}^{0n} \times i \int_0^{\infty} \langle f | i_n(t) \rangle e^{i(E_L + \nu_{i0})t - \Gamma_n t} dt$$

where E_L is the energy of the incident light, n the electronic state, μ^{0n} the electronic transition dipole moment, ν_{i0} the vibrational energy of state $|f\rangle$, and $|i_n(t)\rangle$ is the wavepacket corresponding to the time-dependent nuclear wavefunction of electronic state n . The homogeneous broadening is treated phenomenologically using Γ_n . The overlap between the initial and final wavepacket can be obtained analytically using the independent mode displaced harmonic oscillator (IMDHO) method. This model accounts for vibronic coupling effects but solvent effects in the calculations were not included.

For the MPTTFCCBPQT⁴⁺ complex, the lowest excitation was calculated to be at 827 nm. This result is in very good agreement with the experimental band maximum of 810 nm. The S_1 transition is a charge-transfer transition from the HOMO of the complex, which is largely localized on the MPTTF, to the LUMO localized on the CBPQT⁴⁺ bipyridinium rings (Figure S9a). Our previous result^{S5} for the TTFCCBPQT⁴⁺ complex showed that traditional TDDFT functionals like BP86 significantly underestimate this charge-transfer transition energy. For MPTTF⁺, we find the lowest transition to be at 680 nm and corresponds to a HOMO to SOMO transition (Figure S9b). Experimentally, this transition is found to be at 740 nm. We find two strong, low-lying transitions for the MPTTF²⁺ dication with S_1 at 656 nm and S_2 at 636 nm. The second transition is the stronger of the two with an oscillator strength of $f=0.42$ compared with $f=0.22$ for the S_1 transitions. These two transitions are a combination of the HOMO-1 and HOMO to LUMO transitions (Figure S9c). Thus, for the complex and molecules studied here, the LC- ω PBEh functionals predict excitation energies that are in good agreement with experimental values (Figure 1a-c, in the main text).

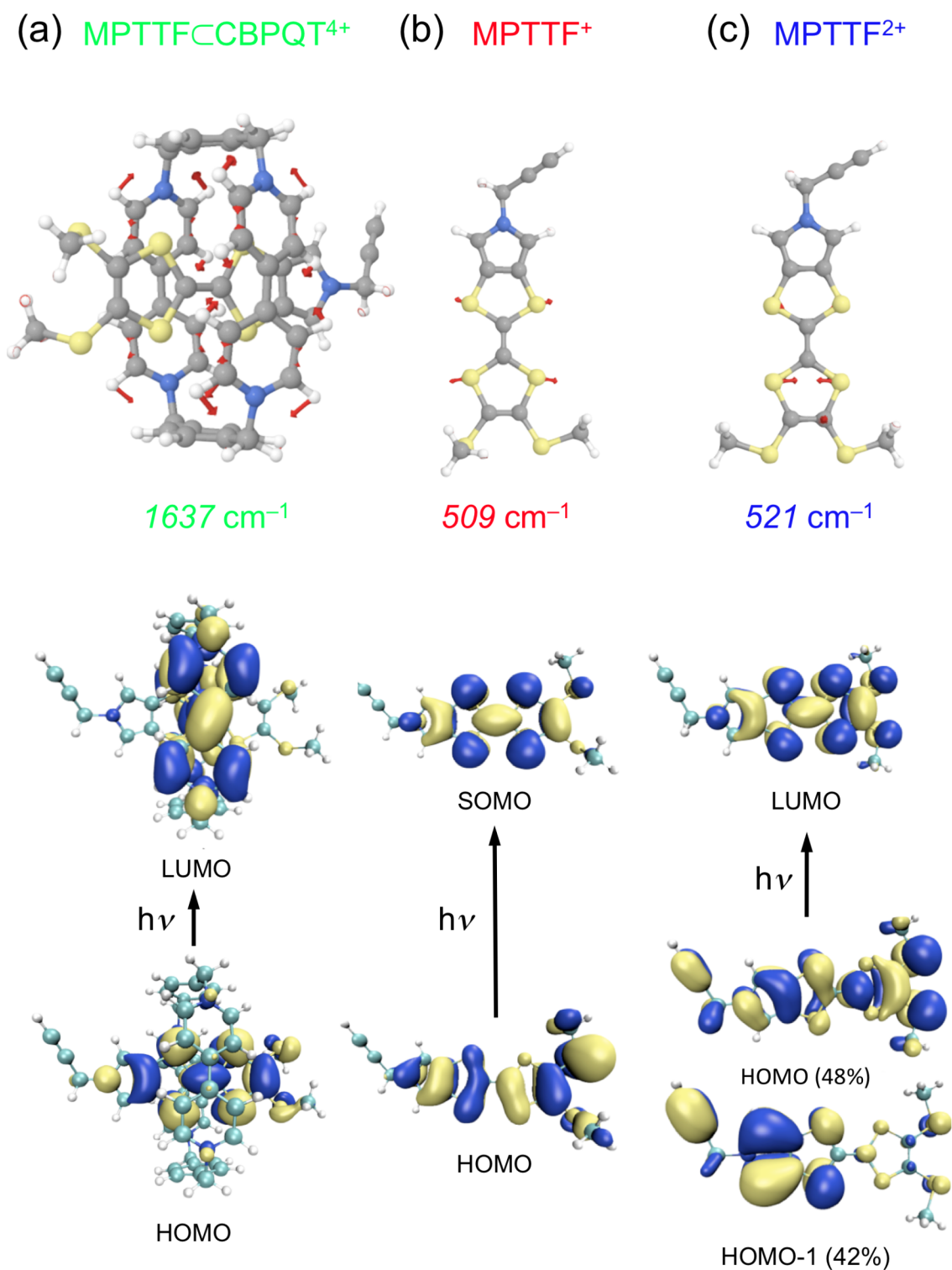


Figure S9. Simulations of the characteristic normal modes (B3LYP, top, red vector arrows indicate atom displacements) and resonant electronic excitations (bottom) for the MPTTFCCBPQT⁴⁺ complex (6-31G*), monocation MPTTF⁺ (6-311G*), and dication MPTTF²⁺ (6-311G*). There is an inter-ring twist angle of 20° for MPTTF²⁺ consistent with the crystal structure of TTF²⁺.^{S11}

The simulated RRS spectra for MPTTFCCBPQT^{4+} , MPTTF^+ , MPTTF^{2+} are shown in Figure S10. The simulations were conducted under resonance with the lowest electronic excited states for each species and using $I = 200 \text{ cm}^{-1}$. Resonance conditions were employed in order to represent an ideal case even though this means the simulations were generated with different excitation wavelengths. For the MPTTF^{2+} dication, the 785 nm excitation used in the experiments is in preresonance with absorption band to the blue. Consequently, the normal Raman spectrum was calculated using a BP86 and a TZP basis set within the ADF program package.^{S12} The BP86 frequencies was scaled for comparison with the B3LYP frequencies.

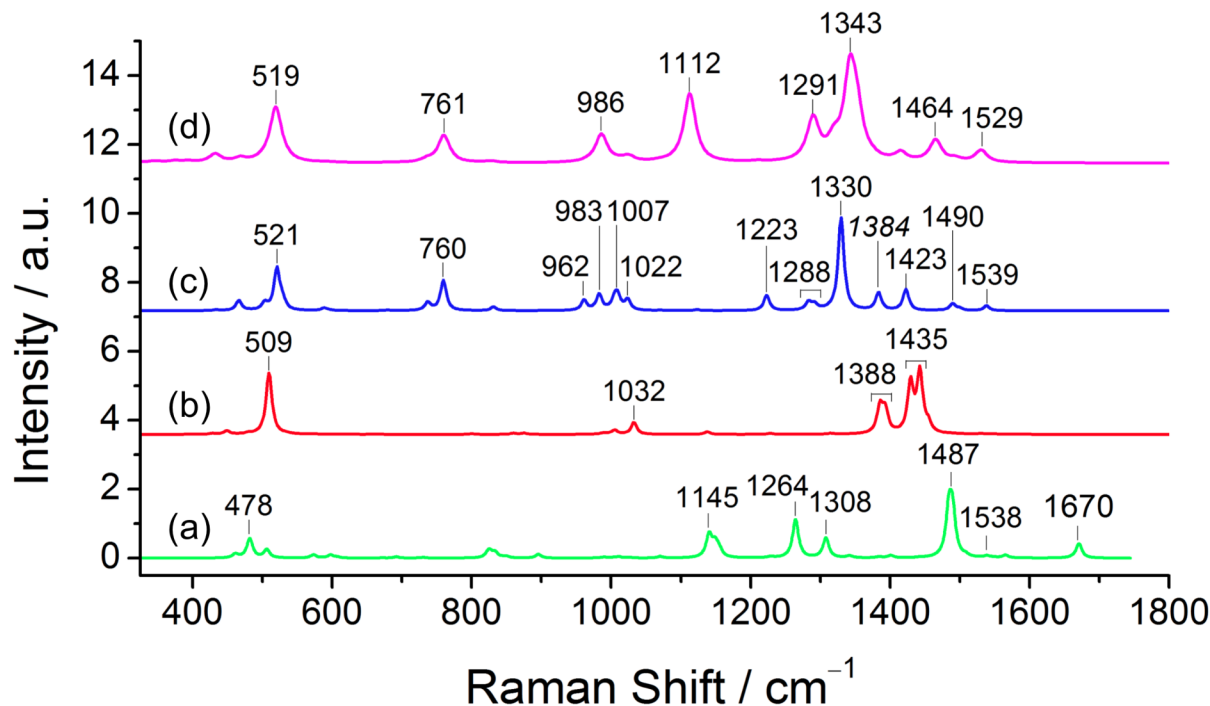


Figure S10. Simulated RRS spectra of (a) MPTTFCCBPQT^{4+} (green), (b) MPTTF^+ (red trace), (c) MPTTF^{2+} (blue) using TDDFT, and (d) the normal Raman spectrum of MPTTF^{2+} (magenta).

Comparing the simulated RRS spectra (Figure S5) for each species with experimental spectra from solution (Figure S4) and from the SERS data (Figure 2 in the main text), we find them in good overall agreement, enabling an assignment of the normal modes for experimental spectra (Figure S9). The modes at 479 cm^{-1} in MPTTFCCBPQT^{4+} , 508 cm^{-1} in MPTTF^+ , and 529 cm^{-1} in MPTTF^{2+} all correspond to the C–S internal stretching mode of the MPTTF unit (the carbon in the C–S vibration originates from the central C=C bond of the MPTTF). As the MPTTF unit gets oxidized, the C–S bond length decreases thus increasing the vibrational frequency. The band at 1640 cm^{-1} in MPTTFCCBPQT^{4+} from the SERRS spectra is assigned to the CBPQT⁴⁺ unit. The monopyrrolo band is found at 1538 cm^{-1} in the simulations (1523 cm^{-1} experimentally). Comparing the normal modes with the molecular orbitals (Figure S9) it is clear that the C–S bonds will change their lengths upon electronic excitation and thus, the C–S stretch is expected to be strongly resonance enhanced. The worst agreement is found for the MPTTF^{2+} where the intensity of the band at 529 cm^{-1} is underestimated compared to the other bands. This is likely a result of preresonance enhancements since this band is already strong in the normal Raman spectrum.

Table S1. Select solution, surface and simulated peak positions^a (cm⁻¹) and relative intensities^b (in italics) for the MPTTF⁺CBPQT⁴⁺ complex.

Solution	Surface	Simulation
1641 <i>(0.004)</i>	1640 <i>(0.08)</i>	1670
	1523 <i>(0.03)</i>	1538
1485 <i>(0.001)</i>	1483 <i>(0.05)</i>	1487
1296 <i>(0.001)</i>	1296 <i>(0.04)</i>	1308
	1246 <i>(0.01)</i>	1264
1157 <i>(0.004)</i>	1157 <i>(0.04)</i>	1145
	478 <i>(0.05)</i>	478

^a Corresponding spectra are found in Figure 2, S4 and S10. ^b Intensities are normalized with respect to the 2253.5 cm⁻¹ solvent band.

Table S2. Select solution, surface and simulated peak positions^a (cm⁻¹) and relative intensities^b (in italics) for MPTTF⁺.

Solution	Surface	Simulation
1933 <i>(0.07)</i>	1934 <i>(0.06)</i>	
1423 <i>(0.46)</i>	1423 <i>(0.30)</i>	1435
507 <i>(0.65)</i>	508 <i>(0.64)</i>	509

^a Corresponding spectra are found in Figures 2, S4 and S10. ^b Intensities are normalized with respect to the 2253.5 cm⁻¹ solvent band.

Table S3. Select solution, surface and simulated peak positions^a (cm⁻¹) and relative intensities^b (in italics) for MPTTF²⁺.

Solution	Surface	Simulation
1330 <i>(0.05)</i>	1330 <i>(0.13)</i>	1330
1299 <i>(0.09)</i>	1296 <i>(0.07)</i>	1288
	1054 <i>(0.03)</i>	
995 <i>(0.08)</i>	994 <i>(0.18)</i>	1007
970 <i>(0.03)</i>	966 <i>(0.08)</i>	983
	843 <i>(0.29)</i>	832
532 <i>(0.70)</i>	529 <i>(1.44)</i>	521
469 <i>(0.02)</i>	466 <i>(0.06)</i>	466

^aCorresponding spectra are found in Figures 2, S4 and S10. ^bIntensities are normalized with respect to the 2253.5 cm⁻¹ solvent band.

S9. Complete References 11b

11b. Anelli, P. L.; Ashton, P. R.; Ballardini, R.; Balzani, V.; Delgado, M.; Gandolfi, M. T.; Goodnow, T. T.; Kaifer, A. E.; Philp, D.; Pietraszkiewicz, M.; Prodi, L.; Reddington, M. V.; Slawin, A. M. Z.; Spencer, N.; Stoddart, J. F.; Vicent, C.; Williams, D. J. *J. Am. Chem. Soc.* **1992**, *114*, 193–218.

S10. References

- S1 (a) Jeppesen, J. O.; Takimiya, K.; Jensen, F.; Becher, J. *Org. Lett.* **1999**, *1*, 1291–1294.
 (b) Jeppesen, J. O.; Takimiya, K.; Jensen, F.; Brimert, T.; Nielsen, K.; Thorup, N.; Becher, J. *J. Org. Chem.* **2000**, *65*, 5794–5805.
- S2 Anelli, P. L.; Ashton, P. R.; Ballardini, R.; Balzani, V.; Delgado, M.; Gandolfi, M. T.; Goodnow, T. T.; Kaifer, A. E.; Philp, D.; Pietraszkiewicz, M.; Prodi, L.; Reddington, M. V.; Slawin, A. M. Z.; Spencer, N.; Stoddart, J. F.; Vicent, C.; Williams, D. J. *J. Am. Chem. Soc.* **1992**, *114*, 193–218.
- S3 Gottlieb, H. E.; Kotlyar, V.; Nudelman, A. *J. Org. Chem.* **1997**, *62*, 7512–7515.
- S4 Vander Griend, D. A.; Bediako, D. K.; DeVries, M. J.; DeJong, N. A.; Heeringa, L. P. *Inorg. Chem.* **2008**, *47*, 656–662.
- S5 Witlicki, E. H.; Hansen, S. W.; Christensen, M.; Hansen, T. S.; Nygaard, S. D.; Jeppesen, J. O.; Wong, E. W.; Jensen, L.; Flood, A. H. *J. Phys. Chem. A* **2009**, *113*, 9450–9457.
- S6 Long, J. R.; Drago, R. S. *J. Chem. Educ.* **1982**, *59*, 1037–1039.

- S7 See Supporting Information from: Witlicki, E. H.; Andersen, S. S.; Hansen, S. W.; Jeppesen, J. O.; Wong, E. W.; Jensen, L.; Flood, A. H. *J. Am. Chem. Soc.* **2010**, *132*, 6099–6107.
- S8 Rohrdanz, M. A.; Martins, K. M.; Herbert, J. M. *J. Chem. Phys.* **2009**, *130*, 054112.
- S9 (a) Govind, N.; Valiev, M.; Jensen, L.; Kowalski, K. *J. Phys. Chem. A* **2009**, *113*, 6041–6043. (b) Jensen, L.; Govind, N. *J. Phys. Chem. A* **2009**, *113*, 9761–9765. (c) Silverstein, D. W.; Jensen, L. *J. Chem. Theo. Comp.* **2010**, *6*, 2845–2855 (d) Bylaska, E. J.; de Jong, W. A.; Govind, N.; Kowalski, K.; Straatsma, T. P.; Valiev, M.; Wang, D.; Apra, E.; Windus, T. L.; Hammond, J.; Nichols, P.; Hirata, S.; Hackler, M. T.; Zhao, Y.; Fan, P.-D.; Harrison, R. J.; Dupuis, M.; Smith, D. M. A.; Nieplocha, J.; Tipparaju, V.; Krishnan, M.; Wu, Q.; Van Voorhis, T.; Auer, A. A.; Nooijen, M.; Brown, E.; Cisneros, G.; Fann, G. I.; Fruchtl, H.; Garza, J.; Hirao, K.; Kendall, R.; Nichols, J. A.; Tsemekhman, K.; Wolinski, K.; Anchell, J.; Bernholdt, D.; Borowski, P.; Clark, T.; Clerc, D.; Dachsel, H.; Deegan, M.; Dyall, K.; Elwood, D.; Glendening, E.; Gutowski, M.; Hess, A.; Jaffe, J.; Johnson, B.; Ju, J.; Kobayashi, R.; Kutteh, R.; Lin, Z.; Littlefield, R.; Long, X.; Meng, B.; Nakajima, T.; Niu, S.; Pollack, L.; Rosing, M.; Sandrone, G.; Stave, M.; Taylor, H.; Thomas, G.; van Lenthe, J.; Wong, A.; Zhang, Z. “NWChem, A Computational Chemistry Package for Parallel Computers, Version 5.1” **2007**, Pacific Northwest National Laboratory, Richland, Washington 99352-0999, USA (a modified version).
- S10 Tannor, D. J.; Heller, E. J. *J. Chem. Phys.* **1982**, *77*, 202–218.
- S11 Ashton, P. R.; Balzani, V.; Becher, J.; Credi, A.; Fyfe, M. C. T.; Mattersteig, G.; Menzer, S.; Nielsen, M. B.; Raymo, F. M.; Stoddart, J. F.; Venturi, M.; Williams, D. J. *J. Am. Chem. Soc.* **1999**, *121*, 3951–3957.
- S12 Baerends, E. J. et al. Amsterdam Density Functional. <http://www.scm.com>